JOURNAL OF PROPULSION AND POWER
Vol. 20, No. 5, September–October 2004

Performance Prediction of a Ducted Rocket Combustor Using a Simulated Solid Fuel

Robert A. Stowe,* Charles Dubois,† and Paul G. Harris‡
Defence R&D Canada–Valcartier, Val-Bélair, Quebec G3J 1X5, Canada
Alfons E. H. J. Mayer§
TNO Prins Maurits Laboratory, 2280 AA Rijswijk, The Netherlands
and
Alain deChamplain¶ and Sophie Ringuette**
Laval University, Québec City, Quebec G1K 7P4, Canada

The ducted rocket is a supersonic flight propulsion system that takes the exhaust from a solid fuel gas generator, mixes it with air, and burns it to produce thrust. To develop such systems, the use of numerical models based on computational fluid dynamics (CFD) has been increasing, but to date only simplified treatments of the combustion within ducted rockets have been reported, likely due to the difficulties in characterizing and accurately modeling the partially reacted, particle-laden fuel exhaust from the gas generator. Through a careful examination of the governing equations and experimental measurements, a CFD-based methodology that properly accounts for the influence of the gas generator exhaust, particularly the solid phase, has now been developed to predict the performance of a ducted rocket combustor using a simulated solid fuel. It uses an equilibrium-chemistry probability density function combustion model with two separate streams, one gaseous and the other of 75-nm-diam carbon spheres, to represent the exhaust products from the gas generator. After extensive validation with direct-connect combustion experiments over a wide range of geometries and test conditions, this CFD-based method was able to predict, within a good degree of accuracy, the combustion efficiency of a ducted rocket combustor.

Nomenclature

C_1	=	diffusion reaction rate constant, kg/(m · s · Pa · K$^{0.75}$)
C_2	=	kinetics reaction rate constant, kg/(m^{2}s · Pa · K)
d_p	=	diameter of particle, m
E_a	=	activation energy, J/kmol
M_{ox}	=	molecular mass of oxidizer
m_{ox}	=	mass fraction of oxidizer
m_p	=	mass of particle, kg
R_1	=	diffusion reaction rate, kg/(m^{2}s · Pa)
R_2	=	kinetics reaction rate, kg/(m^{2}s · Pa)
$\bar{R}$	=	universal gas constant, J/(kmol · K)
T	=	static temperature of surrounding gas, K
T_p	=	temperature of the particle, K
T_{t2}	=	stagnation temperature, end of air inlet diffuser, K
T_{t4}	=	stagnation temperature, end of the combustor, K
t	=	time, s
$\eta_{\Delta T}$	=	efficiency based on temperature rise in the combustor
ρ	=	density, kg/m^3

Subscripts

exp	=	experimental
theo	=	theoretical
∞	=	freestream (far from particle)

Presented as Paper 2001-3461 at the AIAA/ASME/SAE/ASEE 37th Joint Propulsion Conference, Salt Lake City, Utah, 8 July 2001; received 3 June 2003; revision received 4 December 2003; accepted for publication 30 December 2003.

*Leader, Propulsion Group, Precision Weapons Section. Senior Member AIAA.
†Scientist, Energetic Materials Section.
‡Scientist, Propulsion Group, Precision Weapons Section. Member AIAA.
§Scientist, Rocket Technology Group. Member AIAA.
¶Professor, Mechanical Engineering. Member AIAA.
**Graduate Student, Chemistry Department.

Introduction

THE solid fuel ducted rocket, also known as a ramrocket or integral rocket ramjet, is a type of ramjet in which there has been much renewed interest lately for tactical missile propulsion. It has several advantages over solid propellant rocket motors including increased range, higher speed, and throttleability, with only a limited increase in complexity. Once launched, the ducted rocket missile is accelerated to supersonic speed with the integrated solid propellant rocket booster (Fig. 1). When the rocket propellant is completely burned at the end of the boost phase, the port covers that seal the air intakes from the ramjet combustor open and, simultaneously, the gas generator ignites. The effluent from the decomposition of the solid fuel in the gas generator acts as fuel for the ramjet phase of the flight. Because there is little or no oxidizer present in the gas generator, the very fuel-rich effluent includes gases and a substantial portion of condensed-phase material such as solid carbon and, depending on the formulation, metal particles. All of this is injected through the fuel inlet into the ramjet combustor where it is mixed with incoming air, reacts, and is accelerated through a nozzle to provide thrust.

A key component of a ducted rocket missile is the ramjet combustor, and this has been the focus of the current work. It has included literature surveys of computational fluid dynamics (CFD) modeling and experimental work relevant to ducted rockets, water-tunnel visualization and CFD modeling of the nonreacting flow,[1] and direct-connect combustion experiments using a simulated solid fuel based on a mixture of glycidyl azide polymer (GAP) and carbon black.[2] All of these will be presented here briefly. Reacting flow CFD modeling[3] was also carried out with a one-stream probability density function[4] (PDF) combustion model in which the gas generator exhaust, composed of gases and solid carbon, was injected into the combustor as a single homogeneous stream and assumed to react instantaneously with any oxidizer present. This approach, unfortunately, tended to overestimate the combustion efficiency when compared to the direct-connect experiments. To improve these predictions, a two-stream PDF model[5] was used with the gases, and the solid carbon was injected as two separate fuel streams. The solid

Table 1 Geometries and test conditions from previous experiments

Reference	Combustor diameter, mm	Re in combustor	Air inlets and type	Air injection angles, deg	Dome height	Fuel injection type	Stagnation pressure, MPa	Stagnation temperature, K
Clark[6]	196.85	1.85×10^6	2 Circular, 162 deg opposed	60	0.5[a]	In inlets	0.639	610
Choudhury[7]	89	NA	4 Circular, cantable	45, 70	0.6–4.0	Radial central	NA	NA
Zetterström et al.[8]	100	1.16×10^6	4 Circular	60	0.75[a]	In inlets	0.714	704
Stull et al.[9]	150	5.33×10^5	2 Rectangular ventral	30, 45, 60	0.4–0.9	In inlets	0.248	571
Chuang et al.[10] Hsieh et al.[11]	127	8.4×10^5	2 Opposed two dimensional	45	0.48	2 Off-center ports, two dimensional	0.199	286
Dijkstra et al. (TNO-PML)[12]	100	2.16×10^5	2 Circular ventral	45	0.7	Central nozzle protruding 30 mm	0.617	655
Dijkstra et al. (NAWC)[12]	127	2.6×10^5	2 Circular ventral	45	0.96	Central nozzle protruding 51 mm	0.508	653
Ristori et al.[13]	100	1.12×10^6	2 Square, opposed	45	0.65–1.35	2 Nozzles, laterally off center	0.764	527
Schadow[14]	150	2.7×10^5	2 Opposed rectangular slits	45	0, Negative	Central nozzle	0.201	298
Tsujikado et al.[15]	83	4.6×10^5	2 Opposed	75	0.5[a]	Central nozzle	0.464	460
Vigot et al.[16]	85	1.11×10^6	4 Circular, shifted, deflectors	45–90	0.5[a]	Various	NA	NA
Vigot et al.[16]	168	1.76×10^6	4 Circular, shifted, deflectors	45–90	0.5[a]	Various	NA	NA

[a]Estimate.

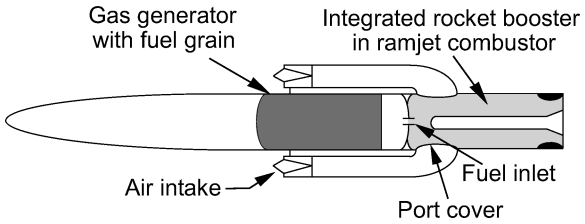

Fig. 1 Components of a ducted rocket.

stream was assumed to consist of 75-nm-diam carbon spheres, which gradually decomposed into carbon monoxide, controlled mainly by surface oxidation, as they flowed through the combustor. The emphasis of this paper is this two-stream PDF model that will not only be compared with the experiments, but also with the earlier one-stream PDF modeling results. Although the combustion modeling was done specifically for a GAP/carbon solid fuel, the overall methodology could certainly be applied to any solid fuel ducted rocket whose gas generator effluent contains both gases and solid particles.

Combustor Configurations and Test Conditions

A review of previous solid fuel ducted rocket tests in the open literature was conducted to yield data on experimental combustor configurations and test conditions (Table 1).[6–16] This information was then used to help develop our own test matrix. All of the configurations were for a side-dump geometry with the air inlets feeding air from the side of the combustor (Fig. 1). This allows the gas generator and fuel injection to be placed adjacent to the head. An alternative to the side-dump geometry is the more compact coaxial center dump geometry, but this is only practical for liquid fuel and solid fuel ramjets that do not use a gas generator. Boundary and test conditions were noted, and additional data were calculated, such as air and fuel velocities, Reynolds numbers based on combustor diameter, and stagnation properties to describe the flow within the combustors more completely. Properties in the combustor were calculated as if the fuel were flowing, but not reacting. The influence of geometry on the flow was examined for all configurations, including the placement of the fuel injector with respect to the airflow. The papers were also examined for additional parameters that described the flow, such as air/fuel velocity, momentum, and mass flow ratios.

The literature survey showed that many different configurations have been investigated. Air inlet injection angles from 30 to 90 deg (Fig. 2) were used, both with and without splitters or guide vanes. Estimated air inlet velocities were up to 200 m/s, with temperatures from ambient to over 700 K and combustor pressures from about 0.2 to over 0.7 MPa. Dome height, given in Table 1 as a fraction

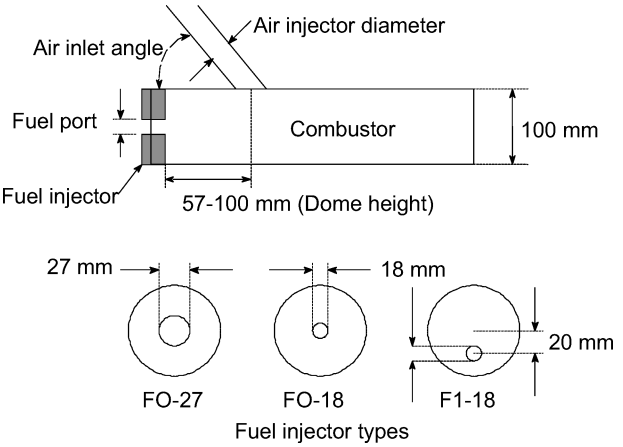

Fig. 2 Schematic of combustor and fuel injectors.

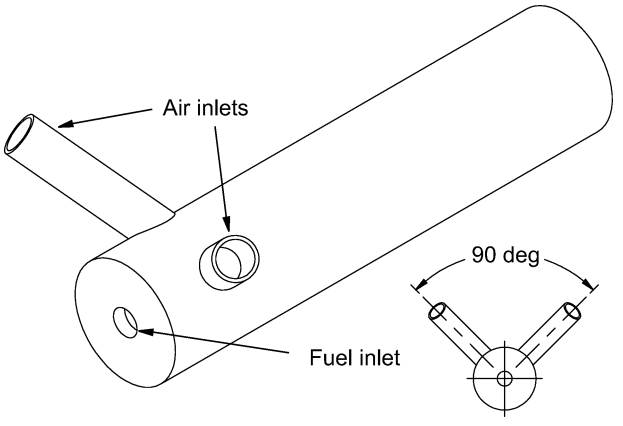

Fig. 3 Basic combustor geometry.

of the combustor diameter, is the axial distance from the head of the combustor to the center of the air inlet(s), as shown in Fig. 2. With a few exceptions, it varied from 40 to 100% of the combustor diameter. For dual-inlet systems, more stable recirculation in the dome region was obtained with the intakes positioned 90 deg apart, as shown in Fig. 3, rather than directly opposed on opposite sides of the combustor at 180 deg. Methods of fuel injection varied widely, from axial to radial when injected from the head, to injection in the air inlets themselves. Impingement of the fuel jet against the air jets was desirable to better break up the fuel jet and improve mixing.

The mixing and the small-scale flow structures in the dome region of the combustor were found to be quite sensitive to geometry and boundary conditions when the fuel was injected from the head, and so this was kept in mind for our own mixing studies. The literature survey also revealed that computer modeling, flow visualization with water tunnels or wind tunnels, and combustion tests (subscale and full scale) were all performed to identify the best configurations and maximize combustion efficiency.

Information from the the literature survey was used to choose a basic geometry (Fig. 3) of dual-inlets spaced 90 deg apart circumferentially, with the main body of the combustor being 100 mm in diameter. The long air inlets would not be practical on a missile, but they were chosen specifically to facilitate testing and the characterization of the boundary conditions. For the direct-connect experiments, the combustor length was deliberately limited to 458 mm, the shortest combustor that could be accommodated within the hardware, so that resulting combustion efficiencies would be relatively low and differences in performance between the configurations would be more obvious. Any calculated efficiencies reported from the reacting flow CFD modeling were also done for this combustor length. A converging/diverging nozzle was mounted at the end of the combustor only for the direct-connect tests so the flow could be choked to build pressure in the combustor; it was neither modeled nor used in the water tunnel experiments because the flows for these were incompressible.

A schematic of the combustor configurations, including the fuel injector geometries, is shown in Fig. 2. The F1-18S fuel injector is similar to the F1-18 fuel injector except that it had its port on the same side as the air inlets rather than opposite to them. The basic geometries of the air injectors are presented in Table 2. Two different dome heights as defined in Fig. 2, 57 and 100 mm, were used.

Previous CFD Combustion Modeling

A literature survey of previous ramjet modeling was carried out and revealed 11 references[13,17–26] on reacting flow modeling in ramjet combustors. The main features of each study are given briefly in Table 3, as well as references[9,10,13,24,26–29] for any experimental data used for comparison. All of the CFD modeling reported used Navier–Stokes (N–S) codes, and most considered only the combustor, but a couple also included part of the inlet and/or the nozzle.

Grids were generally Cartesian and were two and three dimensional. Both incompressible and compressible codes were used. Incompressible formulations were used except when a nozzle was present or there were very high speeds in the air or fuel inlets. The k–ε model was usually used to describe the turbulence, sometimes with modifications to improve its prediction of swirling, recirculating flows. In two cases, an algebraic Reynolds stress model (ASM) was used, but this type of model is much more computationally intensive than the k–ε model and its variants.

For the combustion aspect of the modeling, the trends were from one-step to multistep reactions, from infinitely fast to finite-rate or equilibrium chemistry, and from modeling no influence of the turbulence on the combustion to rigorous modeling of the turbulence/chemistry interaction. Simple hydrocarbon fuels were usually used, and all except one were gaseous. In that one case, liquid kerosene was injected into the flow, and the trajectories and evaporation of the droplets were modeled. There were no studies that took into account the presence of a solid phase, however. To account for the turbulence/chemistry interaction, two basic types of models were used, the first, and older, method being an eddy break-up (EBU) model in which the reaction rate is controlled either by finite-rate chemistry or by turbulent mixing, whichever is slower. The other type of model includes the newer, more complex PDF approach. This type of model can assume that the oxidizer and fuel are completely reacted (mixed is burned), or in equilibrium with possibly some extensions for nonequilibrium effects. The combustion is mixing controlled, and the model is much faster computationally than the EBU model for the same number of species and reactions being considered. The laminar flamelet model (coherent flame example in Table 3) is also a variation of the PDF approach.

The trend was, with time, to use denser grids, newer combustion models, and to move away from in-house, special-use CFD codes toward general-use, commercial codes. For the validation of these modeling methods, only a couple of parametric studies were done to establish grid independence. Any comparison between CFD modeling and experimental results was for the nonreacting flow only, except in a couple of instances where some reacting flow data was available. Unfortunately, none of the reacting flow studies described exactly how combustion efficiency was determined from the CFD results, and usually not even the definition of combustion efficiency was noted.

Table 2 Air injector geometries

Model	Shape of air inlet	Air inlet angle, deg	Air inlet diameter, mm
A2	Circular	60	38.1
A4	Circular	60	50.8
A6	Circular	90	50.8

Direct-Connect Combustion Tests

Information from the literature survey was also used to establish test conditions for the combustion experiments, including the

Table 3 Previous CFD modeling

Reference	Code	Grid	Turbulence model	Combustion model	Fuel	Experimental data
Chen and Tao[17]	Incompressible N–S (TEACH)	Axisymmetric 49 × 15	k–ε	One-step, infinitely fast	Polyester/ammonium perchlorate exhaust	Schadow[27]
Vanka et al.[18]	Incompressible N–S	Three-dimensional, 24 × 11 × 11	k–ε	One-step, infinitely fast, PDF	Ethylene	Stull et al.[9]
Cherng et al.[19]	Compressible N–S	Two dimensional, 30 × 18[a] (estimated)	Modified k–ε	Two-step finite rate, modified EBU	Propane	Chuang et al.[10]
Onn et al.[20]	Compressible N–S	Two dimensional, 32 × 18 (estimated)	Modified k–ε	Two-step finite rate, modified EBU	Propane	Chuang et al.[10]
Yoon and Chung[21]	Compressible N–S	Two dimensional, 40 × 40	Modified k–ε	Two-step finite rate, EBU	Propane	
Hsieh et al.[22]	Compressible N–S, dual-time step	Two dimensional, 99 × 46	Low Re k–ε	One-step finite rate	Propane	
Chao et al.[23]	Compressible N–S	Two dimensional, 40 × 40, adaptive	Modified ASM	Adiabatic PDF	Propane	Chuang et al.[10]
Montazel et al.[24]	Incompressible N–S	Two dimensional, 53 × 24	k–ε	Coherent flame model	Propane	Montazel et al.[24]
Dufour and Montazel[25]	Compressible N–S (CFD–ACE)	Two dimensional	k–ε	Coherent flame model	Propane	Montazel et al.[24]
Liou et al.[26]	Incompressible N–S	Two dimensional, 53 × 29	ASM	One-step finite rate, EBU	Methane	Liou et al.[26]
Dufour and Montazel[25]	Compressible N–S (CFD–ACE)	Three-dimensional, 120,000 cells (full geometry)	k–ε	Coherent flame model	Liquid kerosene (two phase)	Stull et al.[28] Craig et al.[29]
Ristori et al.[13]	Compressible N–S (MSD)	Three-dimensional, 58,060 cells (1/4 geometry)	k–ε	One-step reaction, modified EBU	Propane	Ristori et al.[13]

Table 4 Combustor configurations for direct-connect experiments and combustion CFD modeling

Number	Air injector	Fuel injector	Dome height, mm	Air/fuel momentum ratio	Air/fuel mass ratio	Combustor pressure, MPa	Fuel velocity, m/s	Air velocity, m/s
1	A4	F0-27	57	2.62	7.79	0.396	416	140
2	A4	F0-27	57	11.73	15.73	0.403	328	245
3	A4	F0-27	57	8.89	13.84	0.875	282	181
6	A2	F0-27	57	3.90	7.09	0.411	443	244
7	A2	F0-27	57	19.43	15.76	0.426	311	384
8	A2	F0-27	57	17.94	14.96	0.944	239	287
9	A2	F0-27	57	3.52	6.70	0.845	609	320
11	A4	F0-18	57	4.87	15.36	0.432	710	225
12	A4	F1-18	57	4.07	13.96	0.907	600	175
13	A6	F0-27	57	2.30	7.00	0.44	436	143
14	A6	F0-27	57	10.80	15.33	0.419	324	229
15	A6	F0-27	57	5.20	10.66	0.904	358	175
16	A6	F0-27	57	2.37	7.11	0.8	599	200
18	A4	F0-27	100	2.13	6.65	0.397	501	160
19	A4	F0-27	100	10.93	15.35	0.423	317	226
20	A4	F0-27	100	8.31	13.34	0.882	288	179
21	A4	F0-27	100	2.76	7.62	0.792	564	205
28	A4	F1-18	57	4.84	15.32	0.44	692	219
29	A4	F0-18	57	4.42	14.54	0.917	568	173
30	A4	F1-18S	57	4.29	14.34	0.921	579	173

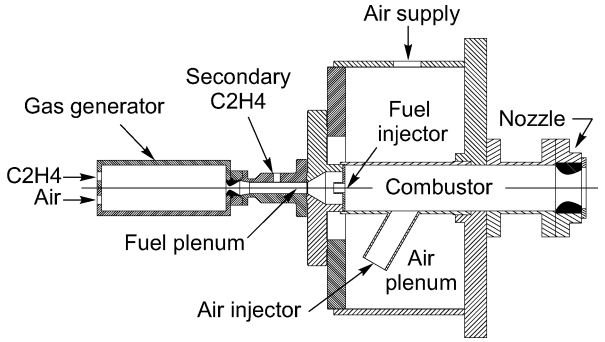

Fig. 4 Ducted rocket hardware.

combustor pressure and the characteristics of the air and fuel flows. Table 4 lists all of the configurations and important test parameters for which both combustion tests and CFD combustion modeling was carried out. Apart from geometry, previous water-tunnel experiments and CFD modeling[1] showed the importance of the momentum ratio of the air- and fuel streams on the flowfield and the mixing; this key parameter is also listed.

All of the combustion experiments were carried out at TNO Prins Maurits Laboratory's direct-connect test facility. High-pressure air was heated by a methane-fueled vitiator to produce stagnation conditions at the combustor representative of those downstream from the air intakes of an actual missile flying at Mach 2.5 and 6000-m altitude (0.5 MPa and 600 K). Additional oxygen was injected at the vitiator to replace that used for the combustion of the methane. A plenum of 0.5-m internal diameter surrounded the air injector to distribute the air as evenly as possible through each of its arms (Fig. 4). This arrangement was chosen to facilitate the changing of the air and fuel injectors and the nozzle at the end of the combustor.

For the solid fuel in the gas generator, a formulation of 90% by mass GAP and 10% carbon was specified and developed. This particular formulation was chosen because GAP will ignite and decompose with no additional oxidizer. Carbon was added to increase its fuel content but maintain an acceptable regression rate. Some direct-connect tests were carried out with this solid fuel, but a single formulation did not give enough flexibility to vary the mass flow rate for the wide range of configurations as proposed. Furthermore, the instantaneous regression rate of a solid fuel is difficult to measure to a sufficient degree of accuracy for these purposes. In the correct proportions, however, the calculated equilibrium exhaust properties of an ethylene/air mixture can be close to those of the GAP/carbon solid fuel.[30] Because the mass flow rates of the ethylene and the air were controlled and measured in the same way as the vitiator gases, the boundary conditions of the effluent injected through the fuel inlet could be estimated with more confidence. The ethylene/air mixture was also much less expensive to use than the solid fuel. All of the results presented here, therefore, use the ethylene/air mixture as the fuel.

However, whereas an actual solid fuel must decompose by itself inside the gas generator once ignited, the mixture of ethylene and air is much too rich to react at the conditions present. About 10% of the ethylene was, therefore, injected into the head of the gas generator, where it reacted with the air in a combustible mixture and flowed through a choked nozzle into the fuel plenum. The remainder of the ethylene was then injected into the fuel plenum, where it could react with the hot exhaust from the gas generator (Fig. 4). The main assumption here, of critical importance to the reacting flow CFD modeling, is that conditions were appropriate to allow the mixture to approach thermochemical equilibrium before being injected into the combustor. Another important point for the CFD modeling is that flow of the reacted ethylene/air mixture was not choked in the fuel inlet before entering the ramjet combustor; the fuel plenum pressure is only slightly higher than the combustor. This arrangement further facilitated the estimation of the fuel inlet boundary conditions and, as to be explained later, meant that the flow could be approximated as being incompressible.

Reacting Flow CFD Modeling

CFD modeling was carried out using FLUENT.[31] A control-volume-based technique is used within FLUENT to discretize the conservation equations for mass and momentum, otherwise known as the Navier–Stokes equations. If required, additional equations for turbulence, species, energy, radiation, and particle tracking can be solved. The segregated solver option was used, which means that the governing equations are solved sequentially. All geometries were modeled as precisely as possible with structured grids of approximately 50,000 hexahedral cells (Fig. 5) for half of the domain (symmetrical about the central longitudinal plane).

Flow in a ducted rocket combustor can be characterized as highly turbulent (Reynolds numbers on the order of 10^6). The renormalized group theory (RNG) model[32] was chosen to model the turbulence because it gives better results than the k–ε model for recirculating, separated flow[31,33] that occurs within a ramjet combustor. Its implementation in FLUENT also includes a correction for swirl. An equilibrium-chemistry PDF approach[31] was chosen to model the reacting flow in the ducted rocket combustor. It is well suited for problems where the fuel and oxidizer inlet streams are separate and the combustion is controlled by turbulent mixing rather than the kinetics of the chemical reactions. With the use of β-shaped PDFs, properties of the reacted mixture anywhere in the combustor can

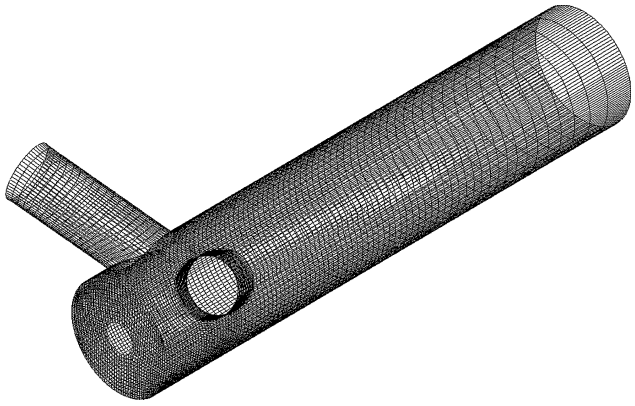

Fig. 5 Surface mesh of basic combustor geometry.

be determined by solving two additional transport equations for the mixture fraction and its variance for each fuel stream. For this approach to give good results, temperatures in the combustor must be high enough so that the characteristic chemical reaction time is short compared to the characteristic mixing time; this is also necessary for the equilibrium chemistry assumption to be valid.

A restriction in FLUENT's implementation of the PDF approach is that the flowfield must be modeled as being incompressible. This is a good assumption in most of the combustor because the Mach number is less than 0.3 almost everywhere. There are exceptions, though. One is the nozzle; it has intentionally not been modelled. The other exceptions are in the air and fuel inlets, where the calculated flow velocities exceed the Mach 0.3 limit for some of the configurations. However, Spalding,[34] states that even flow velocities of up to Mach 0.8 need not be reproduced exactly between a model and a prototype combustor. This implies that the flow in the inlets can be treated as incompressible as long as this higher limit is respected. (It has been exceeded slightly in only a couple of instances for the unchoked flow in the fuel inlets.)

Boundary Conditions

As earlier indicated, the direct-connect hardware and experiments were intentionally set up in such a way as to facilitate the characterization of the boundary conditions for the CFD modeling. For the air inlets, the tubes were lengthened as much as possible within the air plenum and honeycomb installed to straighten the flow and produce a uniform velocity profile at the combustor entrance. Mean velocities at the entrance to the air inlet tubes were calculated from the measured vitiated air mass flow rate and composition, air plenum temperature, and combustor pressure during the direct-connect experiments. Whereas most ramjets with side-mounted inlets have curved inlet ducts, the velocity profiles downstream from these curves depend heavily on the exact geometry. Laser Doppler velocimetry measurements of flow within a plexiglass model of a curved inlet duct,[35] also supplied with air from a large chamber, showed a uniform velocity profile in the lengthy (370-mm) horizontal portion of the duct upstream of the curve, but a nonuniform velocity profile downstream from it. A CFD study of a ducted rocket combustor with a curved inlet diffuser[22] predicted uniform velocity profiles after the normal shock and upstream of the curve in the duct, but nonuniformity downstream from the curve. Therefore, because the air inlet tubes are straight, the desired uniform velocity profiles can be expected throughout, so that this should be a good assumption at the air inlet entrances for the CFD modeling.

Because air from the vitiator arrives at the air plenum in a small-diameter pipe and is suddenly dumped, there should be a significant level of turbulence intensity (where 1% is considered low and over 10% high[31]). Because no measurements of the turbulence characteristics of the air entering the inlets could be made, the turbulence intensity was assumed to be 10%, with a turbulence characteristic length of 25% of the air inlet tube diameter.

Characterizing the fuel inlet boundary conditions was much more challenging. For the air inlets, a constant velocity profile at the fuel inlet was assumed, along with a turbulence intensity of 10% and a turbulence characteristic length 25% of the fuel inlet diameter. For all configurations, measured data from the direct-connect tests, including pressures and temperatures, were used to calculate the measured flow rates and mixture ratio for the ethylene and vitiated air. Table 5 shows the equilibrium exhaust compositions, calculated with the CET89 thermochemical equilibrium code,[36] of an ethylene/air mixture (1.3823 air/ethylene mass ratio) expanded from a chamber pressure of 1.175 MPa to the ramjet combustor pressure of 0.5 MPa. The critical assumption is that thermochemical equilibrium is reached in the fuel plenum. The best way to validate this assumption would be to sample directly the gases within the fuel plenum and analyze them with gas chromatography.

Table 5 Calculated gas generator exhaust properties, air/ethylene ratio 1.3823

Property	Gas generator	Fuel plenum
Pressure, MPa	1.175	0.5
Temperature, K	1274.33	1132.07
Mass fractions		
Ar	0.00829	0.00828
CH_4	0.02354	0.02786
CO	0.24107	0.21598
CO_2	0.00519	0.01329
HCN	0.00008	0.00002
H_2	0.05421	0.05208
H_2O	0.01095	0.02043
NH_3	0.00029	0.00022
N_2	0.41620	0.41628
C(graphite)	0.24020	0.24555
Total	1	1

A parametric study[37] was carried out to determine the consequences of any errors in the estimates of the boundary conditions (including the fuel inlet), or how the combustor was modeled. No significant effects on the predicted efficiency based on temperature rise in the combustor, $\eta_{\Delta T}$, at 458-mm combustor length were seen when heat transfer from the walls, radiation, temperature-dependent transport properties, or a doubled turbulence length scale were included in the CFD model. Doubling the grid in each direction (450,000 cells total), which reduces numerical diffusion and has the same effect as reducing mixing, lowered $\eta_{\Delta T}$ by about 3%. The use of Reynolds stress model for turbulence, second-order discretization, or applying a 10% variation in fuel (gas generator exhaust) temperature, ethylene mass flow rate, or air mass flow rate, all had effects of less than 7%. Using the k–ε turbulence model changed $\eta_{\Delta T}$ by 17%, but this turbulence model is known not to perform as well as the RNG model in this type of flow.[31,33] However, decreasing the turbulence intensity from 10 to 1% or raising it from 10 to 20% had the largest effect, with a 25% change in $\eta_{\Delta T}$. Higher levels of turbulence intensity increased combustion efficiency, as expected.

Two-Phase Flow

For the combustion modeling results previously reported,[3] the boundary conditions for each experiment were used to generate single fuel stream PDF data. This means that all of the fuel, including both the gaseous and solid phases, was injected into the combustor as a single homogeneous stream. The solid carbon was, therefore, assumed to react instantaneously, as were the gases, once there was any oxidizer present. Although a few of the calculated temperature-based combustion efficiencies with the single fuel stream or one-stream PDF were in agreement with the experimental results, most of them were higher. However, bright orange-yellow exhaust plumes, a likely indication of soot particles and incomplete combustion, were observed for some of the direct-connect experiments. This indicates that the soot particles were too large to be assumed to react instantaneously, and this can explain the overprediction of the combustion efficiencies. Therefore, when a two-stream PDF approach,[31] was used with one stream consisting of the gaseous phase and the second consisting of solid carbon soot particles that decompose and

release fuel as they flow through the combustor, improvements to the predictions of combustion efficiency were possible.

The first step to develop a model to describe the motion and decomposition of the particles was to collect and measure some of the solid material during an actual direct-connect combustion experiment. This was accomplished by trapping some of the material from the fuel plenum in an in-line filter. This material was then dispersed in some ethanol using an ultrasonic bath and analyzed in a Malvern Mastersizer 2000. The resulting size distribution, which assumes that the particles are spherical, is shown in Fig. 6. A wide range of particles was detected, from below 0.1 μm to above 200 μm. For comparison, the results from a sample of effluent from a GAP/carbon gas generator are also displayed and show that the ethylene/air fuel can also approximate the particle size distribution of the solid fuel exhaust fairly well between 1 and 200 μm.

Soot from typical hydrocarbon/air combustion consists of minute carbon spheres usually less than 60 nm in diameter. These spheres are grouped together as much larger agglomerates that can be as large as several micrometers (Ref. 38). A scanning electron microscope (SEM) image of the soot collected from the fuel plenum of the reacted ethylene/air mixture is presented in Fig. 7. There are some smooth particles on the order of 1 μm in diameter, but the majority of the collected material has a rough texture and, on closer inspection, is composed of agglomerates made up of spheres of about 75 nm in diameter, a size close to that reported for soot from typical hydrocarbon flames.

Whereas the trajectories of the particles are closely related to their mass and overall dimensions, their decomposition is a function of their total surface area exposed to the oxidizer. This total surface area is related more to the number and diameter of the minute spheres that make up each soot particle rather than the overall size of the particle. To determine the sensitivity of the size of the particles on their trajectories, two-stream PDF modeling (with the subsequently described particle model) for configuration 1 (Table 4) was carried out for a wide range of particle sizes. The trajectories of the particles injected from the fuel inlet hole were calculated using a Lagrangian reference frame,[31] and stochastic particle tracking so that the effects of turbulent fluctuations from the flowfield were included. The continuous-phase flowfield and dispersed- (solid-) phase calculations were coupled, meaning that, not only did the flowfield affect each particle's trajectory and decomposition, but each particle could also affect the flowfield.

The results for the trajectories of these various particle sizes and how much they decompose are shown in Fig. 8. The density of each particle is indicated by its shade of gray. In the side views of the trajectories, the particles from 1 nm to 1 μm diameter appear to fill the bottom half of the combustor and abruptly change direction when deflected by the incoming air jets, and the ensembles of their trajectories appear similar. The 10- and 100-μm particles, however, do not seem to follow the flow as faithfully and have much straighter trajectories toward the end of the combustor. Also, the smaller the particle is, the faster it decomposes. In fact, for the 1-nm particles, about half decompose completely before reaching the end of the combustor. About 10–20% of the 10-nm particles and less than 5% of the 75-nm particles decompose completely before the end of the combustor. For particle diameters of 1 μm and above, all of the particles leave the combustor before they decompose completely.

The results from Fig. 8, therefore, imply that all of the particles can be modeled as 75-nm spheres with little consequence on their average trajectories, particularly for those from 1 nm to over 1 μm in diameter. This is probably valid for the larger particles as well. Because they are of irregular shape, they would have higher aerodynamic drag than spheres of equivalent overall diameter and should follow the flow like the 1-μm-diam and smaller particles. Furthermore, because they are agglomerates, they likely break up as well.

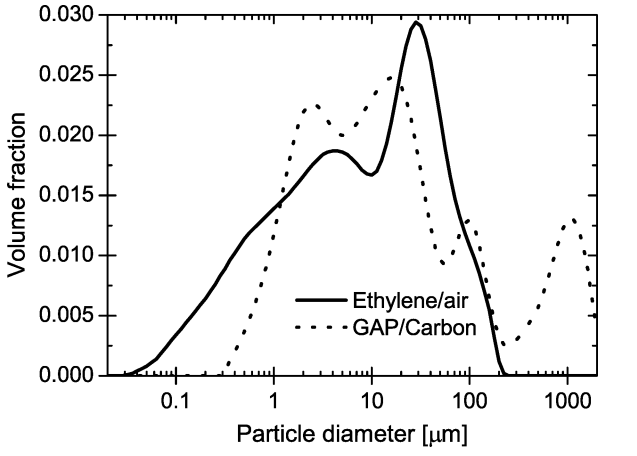

Fig. 6 Particle sizes of ethylene/air and GAP/carbon fuels.

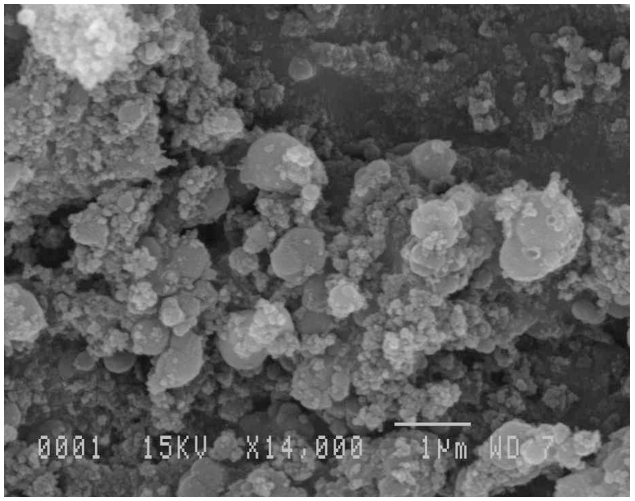

Fig. 7 SEM picture of agglomerated soot particles in the ethylene/air fuel.

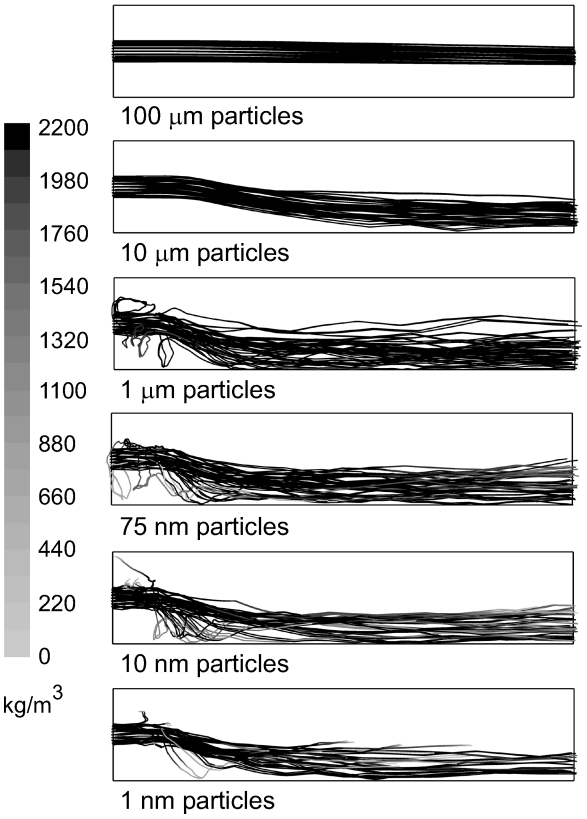

Fig. 8 Predicted particle trajectories vs diameter, configuration 1, side view; scale is particle density.

A kinetics/diffusion model in FLUENT[31] was used to describe the decomposition of the carbon particles. The change in mass of the particles is described by

$$\frac{\mathrm{d}m_p}{\mathrm{d}t} = -\pi d_p^2 \frac{\rho \bar{R} T m_{\mathrm{ox}}}{M_{\mathrm{ox}}} \frac{R_1 R_2}{R_1 + R_2} \tag{1}$$

where ρ and T are the density and temperature of the surrounding gas, m_{ox} and M_{ox} are the mass fraction and the molecular mass of the oxidant in the surrounding gas near the particles, and R_1 and R_2 are the diffusion controlled and the surface kinetics controlled rates, respectively. The diffusion-controlled decomposition rate is derived from an expression for pulverized coal char particles over a wide range of temperatures, where the particles give off carbon monoxide rather than carbon dioxide[39]

$$R_1 = C_1 \left\{ [(T_p + T_\infty)/2]^{0.75} \big/ d_p \right\} \tag{2}$$

where $C_1 = 4.993\,868 \times 10^{-12}$ kg/(m · s · Pa · K$^{0.75}$) and T_∞ is the temperature of the surrounding gas not influenced by the particle. The kinetics of the surface reaction come from an approximation[40] to the Nagel–Strickland-Constable formula for soot oxidation[41] at temperatures below approximately 2000 K:

$$R_2 = C_2 \exp(-E_a/\bar{R}T_p) \tag{3}$$

where $C_2 = 1.11531 \times 10^{-3}$ kg/(m^{2}s · Pa) and $E_a = 1.42537 \times 10^8$ J/kmol is the activation energy of the surface reaction. Because the particle gets very small, the diffusional rate R_1 becomes very large, and the decomposition of the particles becomes controlled by the surface reaction rate. For particles of 75 nm diameter, the decomposition is essentially controlled by the surface reaction rate.

An important feature of the particle decomposition model is that rather than having each particle decrease in diameter as its mass decreases the diameter remains the same while the density decreases. The particle, therefore, becomes more porous. Also, approximately 500 particles had to be injected every 10 flowfield iterations to attain a quasi-steady state and convergence after several hundred iterations. (For clarity, Fig. 8 shows the paths of only 30 of these particles.)

Results

The purpose of the two-stream PDF model was to model more accurately the distribution and decomposition of the solid carbon in the gas generator exhaust and hopefully reduce the overprediction of the temperatures that occurred with the one-stream model. The success of this approach will be shown later. An example of how the two-stream model can change the distribution of temperature in the combustor is shown in Fig. 9. Along the centerline longitudinal axis (a position arbitrarily chosen) for configuration 1, the two-stream model shows a higher heat release than the one-stream approximately 100 mm downstream of the fuel injector. After 150 mm, however, the one-stream model has a higher heat release on the centerline axis, likely due to the two-stream model's solid particles being carried to the bottom of the combustor, as shown in Fig. 8, where they release heat below the centerline.

To show the improvement of the two-stream model over the one-stream model in predicting combustor performance, the results were compared with the results from the direct-connect experiments for all configurations listed in Table 4. The chosen measure to express combustor performance is the efficiency based on temperature rise in the combustor:

$$\eta_{\Delta T} = \frac{T_{t4,\mathrm{exp}} - T_{t2}}{T_{t4,\mathrm{theo}} - T_{t2}} \tag{4}$$

For the direct-connect experiments, the combustion efficiency was estimated using the methods recommended by AGARD.[42] T_{t2} is the air inlet stagnation temperature, and $T_{t4,\mathrm{exp}}$ is the stagnation temperature at the end of the combustor. $T_{t4,\mathrm{exp}}$ is determined from static pressure measurements in the combustor and calculations of theoretical temperatures and characteristic velocities from the CET89 thermochemical equilibrium combustion code. For the CFD results, $T_{t4,\mathrm{exp}}$ is the mass-averaged stagnation temperature at the 458-mm cross section of the combustor to correspond with the length of the combustor for the direct-connect experiments. For both the direct-connect and the CFD results, $T_{t4,\mathrm{theo}}$ is calculated from CET89 using the static pressure in the combustor, the nozzle entrance-to-throat area ratio and the compositions, temperatures, and mass flow rates of the vitiated air and gas generator exhaust as inputs.

A rigorous analysis[37] was also performed to estimate the overall uncertainty for the direct-connect tests. The uncertainties for the mass flow rates of air, at ±2%, and ethylene, at ±5%, had the largest effects on this overall uncertainty. Although the overall uncertainty varied for each configuration, the average value was estimated at ±13% of the value reported for the combustion efficiency. Whereas this may seem high, there is, unfortunately, little in the cited literature with which to compare it. The only comprehensive description of uncertainty analysis for direct-connect testing found in the literature,[43] gave values of overall uncertainty and explained how they were generated based on basic measurement parameters, such as the mass flow rate of air, reported elsewhere[42] for a single test case. Although their estimates of overall uncertainty for $\eta_{\Delta T}$ were lower than ours, so were their uncertainties for almost all of the basic measurement parameters. As stated earlier, a significant amount of our overall uncertainty also came from estimating the exact composition of our ethylene/air mixture, which is not an issue with most of the other testing reported. The reproducibility of our experiments was very good, and results for each of the four repeated configurations differed by much less than the experimental uncertainty. Nonetheless, we are improving the accuracy of our basic measurement parameters.

Figure 10 shows the calculated temperature-based combustion efficiency results for the experiments and the one-stream and two-stream PDF models for the configurations shown in Table 4.

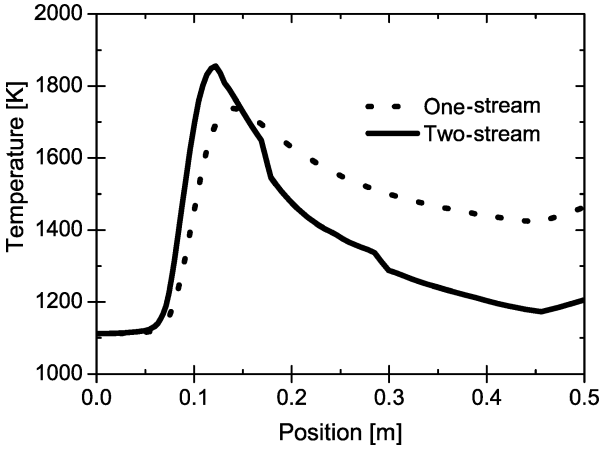

Fig. 9 Predicted temperature distributions on centerline axis, configuration 1.

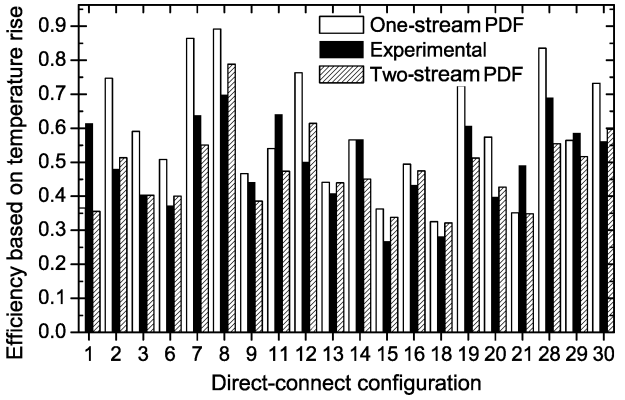

Fig. 10 Results for the calculated efficiencies from the experiments and CFD modeling.

Under careful scrutiny, the one-stream PDF model can be seen to overpredict combustion efficiency for several of the configurations, as previously reported.[3] However, the two-stream PDF model improves the prediction of combustion efficiency for most of the configurations. In fact, the average difference between the two-stream and experimental results is 16%, or nearly the same as the experimental uncertainty, whereas it is 27% between the one-stream and experimental results. Furthermore, with the two-stream model, exactly half of the configurations are overpredicted and the remainder underpredicted, rather than being consistently overpredicted as with the one-stream model.

Although the two-stream PDF model improves the agreement between the experiments and the predictions significantly over the one-stream PDF model, there are still large differences in the results for some of the configurations. An explanation for this may be that the CFD modeling gives a time-averaged output of the flowfield, whereas the flowfield in the experimental combustor is unsteady (as seen in the previous water tunnel visualization[1]) and results in pressure oscillations that are not considered in the model. We carried out some additional tests, done after all of the others listed in Table 4, to determine whether or not there were any combustion-driven waves. However, we had to extend the combustor outside the air plenum (total combustor length 763 mm) so that two water-cooled piezoelectric pressure transducers could be flush mounted to the inner combustor wall just ahead of the nozzle. The transducer signals were sampled at 80 kHz. Because the changing of the length of the combustor will change its acoustics, the goal of these tests was not to determine the exact nature of any combustion instabilities (longitudinal, radial, tangential, which harmonics, etc.) nor identify those due to interactions with the air plenum, gas generator, fuel plenum, etc. (which would have required the careful placement of even more transducers). These tests were simply to confirm the presence of combustion-driven oscillations.

Figure 11 shows the magnitude of the pressure oscillations from one of the transducers vs time. The magnitude of the pressure oscillations due to flow noise, about 50 kPa, can be seen before the spike from the ignition of the gas generator that occurs at 3.0 s. Shortly afterward at about 3.3 s, the fuel-rich exhaust from the gas generator and the vitiated air ignites in the ramjet combustor, and the magnitude of the pressure oscillations doubles to about 100 kPa. At approximately 25% of the average static pressure in the combustor of 0.42 MPa, the magnitude of the oscillations during combustion is indeed significant.

Whereas the magnitude of the oscillations obviously changes before and after ignition of the mixture in the ramjet combustor, fast Fourier transform (FFT) analysis of the signal was done at 1-s intervals to see if the frequencies of the oscillations and the magnitude of each frequency also change. Figure 12 shows that at 2.0 s, before ramjet ignition, there are two significant frequencies at 520 and 2890 Hz. Figure 13 shows an FFT at 6.0 s, well after ramjet ignition, and the frequencies and magnitudes have changed significantly. There are dominant frequencies at approximately 250, 800, 920, 1500, 2420, and 4820 Hz, some of which may be harmonics of the others. The magnitude of the lowest frequency component has also doubled with respect to the 520 Hz peak at 2.0 s. The peak at 250 Hz probably corresponds to the fundamental longitudinal mode in the combustor for a temperature of approximately 1800 K. The same mode before ignition would be at a lower frequency (about 150 Hz) but this was not seen.

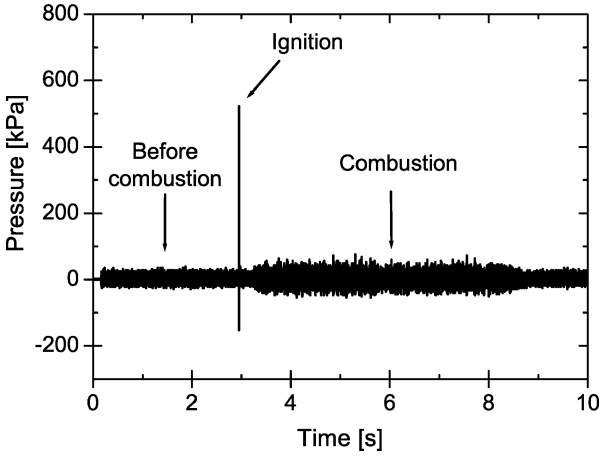

Fig. 11 Pressure variation vs time.

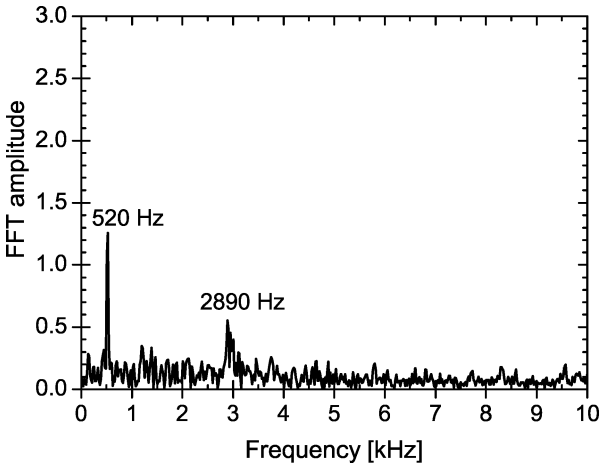

Fig. 12 FFT amplitude vs frequency at 2.0 s.

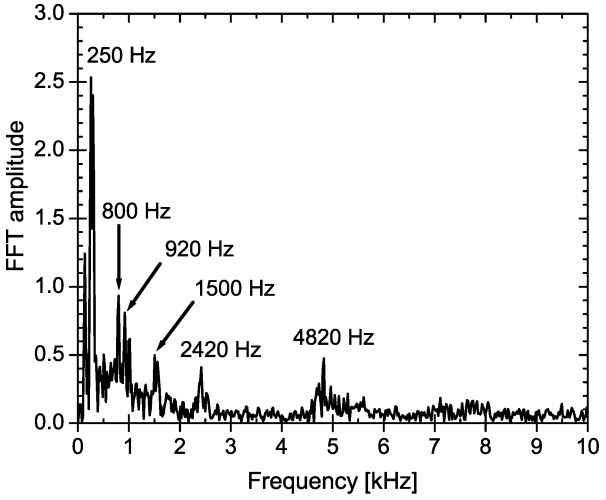

Fig. 13 FFT amplitude vs frequency at 6.0 s.

Apart from showing that the combustor pressure oscillations can be significant, these data have demonstrated that the magnitude and frequency of the pressure oscillations change when combustion occurs in the ramjet and that there is a strong possibility that they are coupled to the combustion processes taking place. The effect of these pressure oscillations on combustor performance has not been considered in the CFD modeling and, therefore, may help explain differences between the experimental and predicted results. Although time-dependent CFD modeling is possible in theory and could take these oscillations into account, this type of modeling would not have been practical for the three-dimensional, turbulent reacting flowfield of interest here.

Conclusions

A CFD-based methodology has been developed to predict the performance of a ducted rocket combustor that uses a simulated solid fuel. It differs from previous methodologies in that it uses a two-stream equilibrium-chemistry PDF combustion model in which the gaseous and solid particle components of the gas generator exhaust are treated separately. It has now been extensively validated with results from direct-connect experiments over a wide range of

configurations and test conditions and can predict, within a good degree of accuracy, the performance of a ducted rocket combustor using a simulated solid fuel.

Modeling the combustion using a two-stream PDF model rather than a one-stream PDF model improved predictions of temperature-based combustion efficiency significantly. The average difference between the two-stream model predictions with the direct-connect experimental results was 16%, or slightly higher than the experimental uncertainty. For the one-stream PDF model, this difference was 27%.

Not properly modeling pressure oscillations in the combustor may account for not being able to predict combustion efficiency accurately for some of the configurations. Pressure oscillations of 25% of the mean static pressure in the combustor were recorded, and FFT analyses suggest that they might be coupled to the combustion processes.

With appropriate changes to the combustion model for different particle sizes and compositions, this methodology could certainly be extended to a wide variety of solid ducted rocket fuels, including metallized formulations.

References

[1]Stowe, R. A., De Champlain, A., Mayer, A. E. H. J., and Niemeijer, S. F., "Modelling and Flow Visualization of Mixing in a Ducted Rocket Combustor," AIAA Paper 98-3768, July 1998.

[2]Mayer, A. E. H. J., and Stowe, R. A., "Experimental Study Into Mixing in a Solid Fuel Ducted Rocket Combustion Chamber," AIAA Paper 2000-3346, July 2000.

[3]Stowe, R. A., De Champlain, A., and Mayer, A. E. H. J., "Modelling Combustor Performance of a Ducted Rocket," AIAA Paper 2000-3728, July 2000.

[4]Kuo K. K., *Principles of Combustion*, Wiley, Toronto, ON, Canada, 1986, Chap. 7.

[5]Stowe, R. A., Dubois, C., Harris, P. G., Mayer, A. E. H. J., De Champlain, A., and Ringuette, S., "Two Phase Flow Combustion Modelling of a Ducted Rocket," AIAA Paper 2001-3461, July 2001.

[6]Clark, W. H., "Experimental Investigation of Pressure Oscillations in a Side Dump Ramjet Combustor," *Journal of Spacecraft and Rockets*, Vol. 19, No. 1, 1982, pp. 47–53.

[7]Choudhury, P. R., "Characteristics of a Side Dump Gas Generator Ramjet," AIAA Paper 82-1258, June 1982.

[8]Zetterström, K.-A., Sjöblom, B., and Jarnmo, A., "Solid Ducted Rocket Engine Combustor Tests," International Symposium on Air Breathing Engines, ISABE Paper 83-7001, 1983.

[9]Stull, F. D., Craig, R. R., Streby, G. D., and Vanka, S. P., "Investigation of a Dual Inlet Side Dump Combustor Using Liquid Fuel Injection," AIAA Paper 83-0420, Jan. 1983.

[10]Chuang, C. L., Cherng, D. L., Hsieh, W. H., Settles, G. S., and Kuo, K. K., "Study of Flowfield Structure in a Simulated Solid-Propellant Ducted Rocket Motor," AIAA Paper 89-0011, Jan. 1989.

[11]Hsieh, W. H., Chuang, C. L., Yang, A. S., Cherng, D. L., Yang, V., and Kuo, K. K., "Measurement of Flowfield in a Simulated Ducted Rocket Combustor Using Laser Doppler Velocimetry," AIAA Paper 89-2789, July 1989.

[12]Dijkstra, F., Mayer, A. E. H. J., Smith, R. A., Wilson, K. J., and Schadow, K. C., "Ducted Rocket Combustion Experiments at Low Gas Generator Combustion Temperatures," AIAA Paper 95-2415, July 1995.

[13]Ristori, A., Heid, G., Cochet, A., and Lavergne, G., "Experimental and Numerical Study of Turbulent Flow Inside a Dual Inlet Research Ducted Rocket Combustor," 14th International Symposium on Air Breathing Engines, ISABE Paper 99-7182, Sept. 1999.

[14]Schadow, K. C., "Boron Combustion Characteristics in Ducted Rockets," *Combustion Science and Technology*, Vol. 5, 1972, pp. 107–117.

[15]Tsujikado, N., Kashikawa, I., Harada, T., and Dohke, K., "Static Firing Tests of Experimental Ram-Rocket with Highly Boron Loaded Solid Propellant Type Fuels," International Symposium on Air Breathing Engines, ISABE Paper 87-7028, 1987.

[16]Vigot, C., Cochet, A., and Guin, C., "Combustion Behaviour of Boron-Based Solid Propellants in a Ducted Rocket," *Combustion of Boron-Based Solid Propellants and Fuels*, CRC Press, Boca Raton, FL, 1993, pp. 386–401.

[17]Chen, L., and Tao, C. C., "Study on the Side-Inlet Dump Combustor of Solid Ducted Rocket with Reacting Flow," AIAA Paper 84-1378, June 1984.

[18]Vanka, S. P., Craig, R. R., and Stull, F. D., "Mixing, Chemical Reaction, and Flowfield Development in Ducted Rockets," *Journal of Propulsion and Power*, Vol. 2, No. 4, 1986, pp. 331–338.

[19]Cherng, D. L., Yang, V., and Kuo, K. K., "Numerical Study of Turbulent Reaction Flows in Solid-Propellant Ducted Rocket Combustors," *Journal of Propulsion and Power*, Vol. 5, No. 6, 1989, pp. 678–685.

[20]Onn, S. C., Chiang, H. J., Hwang, H. C., Wei, J. K., and Cherng, D. L., "Optimization of Operation Conditions and Configurations for Solid-Propellant Ducted Rocket Combustors," AIAA Paper 93-1885, June 1993.

[21]Yoon, W. S., and Chung, T. J., "Numerical Simulations of Airbreathing Combustion at All Speed Regimes," AIAA Paper 93-1972, June 1993.

[22]Hsieh, S. Y., Yang, V., Cherng, D. L., and Yang, H. T., "A Unified Flow Analysis of Ramjet Propulsion Systems," AIAA Paper 94-3326, June 1994.

[23]Chao, Y. C., Chou, W. F., and Liu, S. S., "Computation of Turbulent Reacting Flow in a Solid-Propellant Ducted Rocket," *Journal of Propulsion and Power*, Vol. 11, No. 3, 1995, pp. 473–482.

[24]Montazel, X., Samaniego, J. M., Lacas, F., Poinsot, T., and Candel, S., "Turbulent Combustion Modelling in a Side Dump Ramjet Combustor," AIAA Paper 92-3599, July 1992.

[25]Dufour, E., and Montazel, X., "Numerical Simulation of Direct Connect Liquid-Fueled Ramjet Tests," AIAA Paper 98-3769, July 1998.

[26]Liou, T. M., Chen, L., and Wu, S. M., "Effects of Momentum Ratio on Turbulent Nonreacting and Reacting Flows in a Ducted Rocket Combustor," *International Journal of Heat and Mass Transfer*, Vol. 36, No. 10, 1993, pp. 2589–2599.

[27]Schadow, K. C., "Experimental Investigation of Boron Combustion in Air-Augmented Rockets," *AIAA Journal*, Vol. 7, No. 10, 1969, pp. 1870–1876.

[28]Stull, F. D., Craig, R. R., and Hojnacki, J. T., "Dump Combustor Parametric Investigation," Rept. AFAPL-TR-74-90, Air Force Aero Propulsion Lab., Wright–Patterson Air Force Base, Nov. 1974.

[29]Craig, R. R., Drewry, J. D., and Stull, F. D., "Coaxial Dump Combustor Investigation," AIAA Paper 78-1107, July 1978.

[30]Dijkstra, F., "Conceptual Design of a Ducted Rocket Combustor," M.S. Thesis A2R-P21, Faculty of Aerospace Engineering, Delft Univ. of Technology, Delft, The Netherlands, 1993.

[31]"FLUENT 5 User's Guide," Fluent, Inc., Lebanon, NH, 1998.

[32]Yahkot, V., Orszag, S. A., Thangham, S., Gatski, T. B., and Speziale, C. G., "Development of Turbulence Models for Shear Flows by a Double Expansion Technique," *Physics of Fluids A*, Vol. 4, No. 7, 1992, pp. 1510–1520.

[33]Ferreira, A., Sousa, A. C. M., Viegas, D. X., "Numerical Tests of the k–ε and RNG Turbulence Models for the Flow Around a 3D Surface Mounted Obstacle," *Proceedings of the Ninth Annual Conference of the CFD Society of Canada*, CFD Society of Canada, Ottawa, 2001, pp. 524–529.

[34]Spalding, D. B., "The Art of Partial Modeling," *Ninth Symposium on Combustion*, Academic Press, London, 1963, pp. 833–843.

[35]Liou, T. M., and Liao, C. C., "Flows in a Curved Combustor Inlet With and Without a Guide Vane," *Journal of Propulsion and Power*, Vol. 11, No. 3, 1995, pp. 464–472.

[36]McBride, B. J., "CET89—Chemical Equilibrium with Transport Properties," NASA Lewis Research Center, Cleveland, OH, 1989.

[37]Stowe, R. A., "Performance Prediction of a Ducted Rocket Combustor," Defence Research Establishment/Valcartier, Technical Rept. DREV TR 2001-200, Val-Bélair, QC, Canada, Nov. 2001.

[38]Faeth, G. M., and Köylü, U. O., "Soot Morphology and Optical Properties in Nonpremixed Turbulent Flame Environments," *Combustion Science and Technology*, Vol. 108, 1995, pp. 207–229.

[39]Field, M. A., "Rate of Combustion of Size-Graded Fractions of Char from a Low Rank Coal Between 1200K–2000K," *Combustion and Flame*, Vol. 13, No. 3, 1969, pp. 237–252.

[40]Glassman, I., *Combustion*, 2nd ed., Academic Press, Orlando, FL, 1987, Chap. 9.

[41]Nagel, J., and Strickland-Constable, R. F., "Oxidation of Carbon Between 1000–2000°C," *Proceedings of the Fifth Conference on Carbon*, Pergamon Press, New York, 1962, pp. 154–164.

[42]"Analytical Methods for the Determination of Connected-Pipe Ramjet and Ducted Rocket Internal Performance," Propulsion and Energetics Panel Working Group 22 Rept. AGARD-AR-323, AGARD 1994.

[43]Blevins J., and Coleman, H., "Uncertainty Assessment of Ramjet Performance Determination in Connected-Pipe Testing," AIAA Paper 95-3074, 1995.